Review : Referee
Draft
2-6-91

AN INVESTIGATION OF THE IMPACT OF FRACTURE COATINGS ON FRACTURE/MATRIX FLOW INTERACTIONS IN UNSATURATED, POROUS MEDIA *

By

Steven G. Thoma [1]
David P. Gallegos [2] **
Douglas M. Smith [1]

[1] UNM/NSF Center for Micro-Engineered Ceramics
University of New Mexico
Albuquerque, NM 87131

[2] Waste Management Systems
Division 6416
Sandia National Laboratories
Albuquerque, NM 87185

Sandia Control No. SAND91-0355J

Sandia Project Monitor: D.P. Gallegos

Submitted to:

GROUND WATER
Submitted: February 1991

** Author for communications

HYDROLOGY DOCUMENT NUMBER 630

*This work was performed at Sandia National Laboratories, which is operated for the U.S. Department of Energy under contract number DE-AC04-76DP000789.

ABSTRACT

Ground water flow in unsaturated, fractured rock is often assumed to be dominated by the porous matrix component. This is frequently the result of assuming that water flowing in the fractures is imbibed into the matrix by capillary suction forces with negligible resistance to uptake at the matrix-fracture interface. However, the existence of a mineralized layer or coating at this interface may substantially reduce matrix imbibition and consequently result in fracture-dominated flow. To test this idea, four tuff samples containing natural fractures were obtained from tuff formations in southern Nevada. By performing capillary rise experiments into the matrix rock, across a mineralized fracture face and then across a fresh uncoated fracture face, water uptake as a function of time and coating was measured. A relatively simple model has been developed to describe the imbibition behavior. The experimental techniques and imbibition models used were shown to be reliable using ordered sphere packings with known pore size and structure. From the tuff imbibition data, the ratio of the permeability through the mineralized face to the permeability through the uncoated face was found to vary from 0.3 (relatively little effect of the mineralized layer) to 10^{-7} (uptake dominated by the mineralized layer). Using a simple fracture flow model and the imbibition model mentioned above to simulate matrix uptake from the fracture, numerical experiments indicate that the existence of fracture coatings may significantly decrease the travel time and increase the travel depth of water flowing through fractures.

INTRODUCTION

Currently, the proposed site for disposal of commercial high-level radioactive waste in the United States is the Yucca Mountain site located on the southwestern boundary of the Nevada Test site in southern Nevada. The host rock for the proposed repository lies within a series of ash-flow and bedded volcanic tuffs, that are both unsaturated and fractured.

Climate at Yucca Mountain is generally very arid, although high intensity rain storms occur during the summer months. It is thought that during these storms, fracture flow may be initiated. Once fracture flow has begun, water can be imbibed across the fracture face into adjacent porous matrix by capillary suction forces. If, however, the flow across the fracture face is inhibited in some way, then flow down the fracture can continue.

Ground water travel times through the unsaturated zone are much greater under the conditions of matrix-dominated flow than by fracture flow. A matrix-dominated flow situation could provide favorable conditions for a hazardous waste disposal site located in the unsaturated zone in that ground water travel times and therefore, contaminant transport times, may be very long. As a first approximation, travel times are often estimated from the fracture size and spacing, matrix permeability, degree of saturation, and fracture and matrix pressures. Assuming that all fracture flow is imbibed by the matrix requires that the resistance to flow into the matrix across the fracture/matrix interface be negligible. In doing so, the role of an uptake-inhibiting mineralized layer or coating on the fracture face is neglected.

Fractures at Yucca Mountain are generally coated or filled to some extent at all depths, down to and below the water table [Sykes et al., 1979; Spengler et al., 1984; Carlos, 1985; Crowe and Vaniman, 1985; Carlos 1987]. The mineralogy, thickness, and amount of coverage of fracture coatings are highly variable. Whereas some fractures appear to have no coating, others are completely coated or filled. Typical coatings may include manganese oxides, manganates, iron oxides, iron hydroxides, silica, zeolites, smectites, or carbonates [Spengler et al., 1984; Carlos 1985]. Capillary uptake of water by the matrix from the fracture must occur across these mineralized coatings and thus may be potentially inhibited by them.

A mineralized coating on the fracture face might have a permeability much lower than the adjacent matrix, and despite the relatively small coating thickness, effectively insulate the matrix from the fracture. The existence of such a fracture coating could invalidate conceptual models for ground-water flow based on matrix-dominated flow and models assuming negligible fracture/matrix flow resistance. Furthermore, the occurrence of intermittent fracture flow could preclude the use of a continuum approach for ground-water flow modeling.

In this study, we investigate the effect of natural fracture surface coatings on the water uptake rate during capillary rise experiments. Fracture-to-matrix flow is modeled using a Darcy's law/Washburn Equation relationship, which takes into account fracture/matrix interfacial resistance. A series of water-uptake experiments were performed on fabricated model materials, as well as, on tuff samples to test our method and model, demonstrate the

significance of fracture coating resistance to flow, and provide some guidance for obtaining realistic values of the coating resistivity which may then be used to modify existing flow models. Additionally, simple numerical experiments were conducted to investigate the impact of low-permeability fracture coatings on the travel distance of a plug of water moving down a fracture.

To test the validity of using of the Washburn Equation [see Dullien, 1979] for modeling capillary uptake, capillary rise experiments were conducted on a series of compacts made from sub-micron, monodisperse silica spheres with different samples having different packing geometries and sphere sizes. Capillary rise experiments were also performed on compacts that consisted of two distinct, similar length regions in series. Each of the two regions contained distinctly different size spheres and therefore, different pore size distributions. The results of the latter experiment would demonstrate the effect of discrete layers on water uptake behavior. In another set of experiments, imbibition was measured into pellets prepared from monosize spheres which were coated on one end with a silica gel, simulating a porous matrix material covered with a thin, low permeability surface layer (i.e., fracture coating).

To ascertain the effect of a mineralized coating layer on matrix imbibition in natural materials, uptake measurements were made on a series of tuff samples. Uptake was measured through the natural fracture face (coated) and then through a freshly cut matrix face (uncoated) parallel to the natural fracture face. A model that combines Darcy's Law (for flow through the fracture coating) and the Washburn Equation (for flow into the matrix) was used to describe these imbibition results. In all cases, the experimental results were compared with those predicted by the model. By comparing the difference in uptake behavior through the coated fracture surface to the uptake behavior through the uncoated surface, the impact of surface resistivity was assessed.

BACKGROUND

A great deal of work has been conducted to model ground water flow conditions in the unsaturated zone of the Yucca Mountain site [Montazer and Wilson, 1984; Ross, 1984; Travis et al., 1984; Wang and Narasimhan, 1985; Wang and Narasimhan, 1986; Peters et al.,

1986; Lin and Tierney, 1986; Cederberg et al., 1987; Peters and Klavetter, 1988; Zimmerman and Bodvarsson, 1989; Zimmerman and Bodvarsson, 1990]. The flow setting in the unsaturated zone consists of flow through both a partially saturated matrix and through fractures. One of the many difficulties in modeling this type of system is adequately predicting the imbibition behavior of the matrix material at the fracture/matrix interface during fracture flow. Richard's equation has been used to describe the flow of water in an unsaturated porous medium [Dullien, 1979], but analytical solutions are often impractical due to non-linearities which arise from the variation of the permeability and capillary pressure with water content. A number of numerical models have been developed to model flow in both unsaturated and fractured media [for example, Bixler, 1985; Dudley et al., 1988; Hopkins and Eaton, 1990]. However, most of the numerical models treat the system as an equivalent porous medium by assuming that the pressures in the fractures and matrix are equal. Recently, Zimmerman & Bodvarsson [1990] have developed a semi-analytical/semi-numerical model which addresses this problem by use of the van Genuchten [1980] expressions to derive a source-sink term for flow between the fracture and matrix. It is still assumed, however, that there is zero resistance to flow at the matrix/fracture interface. Updegraff and Lee [1991] have developed a numerical model which assumes that the matrix and fracture act as separate continua, and are linked through a transfer term which is a function of the pressures in the fracture and matrix, and a transfer coefficient. So while the analytical difficulty of this situation is being addressed, the effects of matrix/fracture interfacial resistivity have yet to be explored.

THEORY

The topic of capillary uptake in porous media has been the subject of considerable research and is reviewed elsewhere [Dullien, 1979]. The simplest expression commonly used to describe capillary uptake rate is the Washburn equation [as given by Dullien, 1979]:

$$\frac{dh}{dt} = \frac{1}{8\mu h}\left(\frac{2\sigma\cos(\theta)}{r} - \rho g h\right)R^2 \qquad (1)$$

where h is the capillary rise, μ is viscosity, σ is surface tension, θ is the contact angle, r is the pore radius, ρ is liquid density, g is the gravitational constant, and R is r/τ (τ being the tortuosity factor). Equation 1 is based on the assumption that pores are cylindrical,

non-intersecting, and of uniform size. It is accurate for all except very short times [Szekely et al., 1971] and implies the presence of a sharp saturation front. Observations by Van Brakel and Heertjes [1977a; 1977b] also support the use of Equation 1.

The height of capillary rise as a function of time can then be determined (neglecting gravity effects) by integrating Equation 1:

$$h^2 = \frac{\sigma \cos(\theta) t R^2}{2\mu r} = \frac{\sigma \cos(\theta) t r}{2\mu \tau^2} \tag{2}$$

Equation 2 is applicable to a single distinct region and predicts that the height of capillary rise, h, should be a linear function of $t^{1/2}$.

Now consider an element as shown in Figure 1, with two distinct regions, and where P_a, P_i, and P_c are the ambient, interfacial, and capillary pressures, respectively. At time t_1 the level of saturation is at height h_1, and at time t_2, the level of saturation is at height h_2. L_1 is defined to be the height of region 1 and A is the normal cross sectional area of the sample. For uptake through this element when $h_1 < L_1$ (unsaturated flow), the Washburn Equation is applicable and the volumetric uptake can be expressed as:

$$V = A\epsilon_1 \sqrt{\frac{\sigma \cos(\theta) t_1 r_1}{2\mu \tau_1^2}} \tag{3}$$

where ϵ is the porosity. However, when $h_2 > 0$ (saturated flow in region 1), Darcy's Law is applied in region 1:

$$Q = \frac{k_1 A (P_i - P_a)}{\mu L_1} \tag{4}$$

Q is the volumetric flow rate (dV/dt) and k_1 is the permeability of region 1. The Washburn Equation (Equation 2) is then applicable in region 2.

Given Equation 4 and assuming that the pressures in region 2 are related by

$$P_c - P_i = \frac{8\mu h_2}{R_2^2}\frac{dh_2}{dt_2} \tag{5}$$

an expression for P_c - P_a can be derived:

$$P_c - P_a = \frac{Q\mu L_1}{k_1 A} + \frac{8\mu h_2}{R_2^2}\frac{dh_2}{dt_2} \tag{6}$$

In addition, the assumption can also be made that [Washburn, 1921]:

$$P_c - P_a = \frac{2\sigma\cos(\theta)}{r_2} \tag{7}$$

Noting that the volumetric flow rate in region 2 can be expressed as

$$Q = \frac{dV}{dt_2} = \frac{dh_2}{dt_2} A\,\epsilon_2\,, \tag{8}$$

Equations 6, 7, and 8 can be combined and the resulting combination can then be integrated to yield:

$$\frac{\epsilon_2 \mu L_1 h_2}{k_1} + \frac{4\mu h_2^2}{R_2^2} = \frac{2\sigma\cos(\theta)t_2}{r_2} \tag{9}$$

When $h_1 = L_1$, t_2 is defined to be equal to zero (see Figure 1). Therefore, $t_2 = t - t_1$, where t is the total time. This is equivalent to:

$$t_2 = t - \frac{2\mu L_1^2 r_1^2}{\sigma\cos(\theta) r_1} \tag{10}$$

Also recognize that the height of the capillary rise in region 2 is given by

$$h_2 = \frac{\textit{total volume - volume of region 1}}{\textit{area of region 2}} = \frac{V - A\epsilon_1 L_1}{A\epsilon_2} \tag{11}$$

Therefore, Equations 10 and 11 can be substituted into Equation 9 to obtain an expression for volumetric uptake by the sample as a function of time. After simplification, this expression is given as:

$$V^2 + BV + C = Dt \tag{12}$$

where

$$B = \frac{\epsilon_2^2 A r_2^2 L_1}{4\tau_2^2 k_1} - 2A\epsilon_1 L_1$$

$$C = \frac{\epsilon_2^2 A^2 r_2 L_1^2 \tau_1^2}{r_1 \tau_2^2} - \frac{\epsilon_2^2 A^2 r_2^2 L_1^2 \epsilon_1}{4\tau_2^2 k_1} + A^2 \epsilon_1^2 L_1^2 \tag{13}$$

$$D = \frac{\epsilon_2^2 A^2 r_2 \sigma \cos(\theta)}{2\mu \tau_2^2}$$

In terms of a fracture/matrix system, the positive root to the quadratic Equation 12 mathematically describes the time-dependent imbibition of a liquid into an initially dry porous matrix across a coating that has a permeability k_1, thickness L_1, single representative pore size r_1, tortuosity τ_1, and porosity ϵ_1.

Now that an expression is given for the volumetric uptake of water by the porous matrix, across a coated fracture face, the impact of the fracture coating properties on the travel depth of a plug of water moving down a single fracture can be assessed. As depicted in Figure 2, a plug of water with length L_p and width W is flowing down a fracture of aperture 2h. At any given time, the volume of the plug is $2hL_pW$. The flux out of the plug is given by $2L_pWV$, where V is the volumetric uptake of water by the matrix (described by Equation 12). Note that both L_p and V are functions of time. The change in the volume of the plug, V_p, over time is then given by
which, when expressed in terms of the plug length, is equivalent to

$$\frac{dV_p}{dt} = 2L_p W V_{ave} \tag{14}$$

$$\frac{dL_p}{dt} = \frac{L_p V_{ave}}{2h} \tag{15}$$

In Equations 14 and 15, V_{ave} is the average volumetric uptake over a given contact time t_c, and is defined by

$$V_{ave}(t_c) = \frac{\int_0^{t_c} V(t)dt}{\int_0^{t_c} dt} = -\frac{B}{2} + \frac{(B^2 - 4C + 4Dt_c)^{3/2}}{12Dt_c} \tag{16}$$

The contact time, t_c, is the time that a plug of water is in contact with a given point on the fracture face as the plug moves down the fracture. The contact time is defined to be equal to the length of the plug divided by the velocity of the plug vertically downward ($t_c = L_p/v$). Assuming that a fracture acts as two smooth parallel plates, the velocity of such a plug moving down the fracture would be given by

$$v = \frac{h^2}{3\mu L_p}\left(\frac{\sigma\cos(\theta)}{h} - \rho g L_p\right) \tag{17}$$

Note that the capillary forces oppose the gravitational forces and, therefore, tend to slow the plug down. As fracture water is imbibed by the adjacent matrix, the length of the plug will accordingly decrease, until eventually a plug length is reached at which point the capillary forces will equal the gravitational forces. The velocity of the plug at this point equals zero. Also note that as the fracture aperture decreases, the length of a plug of water that it can support by capillary forces increases.

EXPERIMENTAL

Capillary uptake measurements (volume of water imbibed as a function of time) were made on both fabricated (or model) porous media with well-characterized pore structure and flow properties, and a series of tuff samples containing natural fractures. Model porous media were produced using several sizes of monodisperse silica spheres, with each sample

containing a single sphere size. The spheres were synthesized via the hydrolysis and condensation of tetraethyl orthosilicate (TEOS) in ethanol following the method described by Stober et al. [1968]. The sphere diameter was varied by changing the relative concentration of TEOS and ammonium hydroxide in the reaction mass.

Ordered, cylindrical packings of these spheres were produced via centrifugation of sphere dispersions. Packings were prepared from two different sphere sizes (130 and 270 nm sphere diameter), in two different cylinder diameters (0.20 and 0.48 cm). The cylinder lengths were varied between 0.5 and 1.5 cm.

To produce a layered pellet, two sets of spheres were prepared, with mean particle diameters of 100 nm and 345 nm, respectively. Initially, the larger-sphere-diameter powder (0.6 g of powder) was placed in a 3/8 inch diameter, hardened steel die and hand compacted with a steel punch. The smaller-sphere-diameter powder (0.6 g) was then placed in the die on top of the previously hand compacted material. The entire contents were then pressed uniaxially at 10,000 psi to form a firm, coherent sample. The result was 50/50 wt% pellet of these two materials with a distinct boundary between them.

To produce a xerogel [Brinker and Scherer, 1990] coated pellet, 0.5 g of filtered, dried (at 110°C), 270 nm spheres were uniaxially pressed at 10,000 psi. To successfully coat one end of the pellet with an acid catalyzed xerogel, it was necessary to first coat the sample with a layer of smaller diameter spheres. A suspension of 20 nm spheres was prepared (size based on calculations by Stober et al. [1968]), and concentrated to 45% of the original volume via evaporation. Ten drops of the concentrated suspension were spin coated (at 1500-2000 RPM), onto one end of the pellet, after which the pellet was again dried at 110°C for one hour. Next, a xerogel was prepared following the method of Brinker and Scherer [1990]. Xerogels generally have very small pores (< 2 nm) and low permeability. The xerogel solution was diluted to 50% with ethanol, and subsequently applied to the pellet via spin coating. Six successive gel coatings were applied, each coating consisting of 5 drops followed by heat treatment at 110°C for one hour.

Prior to capillary uptake measurements, the pellet and cylindrical packing perimeters were sealed using heat shrink tubing. Uptake experiments were conducted through one end of each of the single-sphere-size cylindrical packings. Uptake through both ends of the two-

layered pellet was measured. Uptake was measured into the uncoated 270 nm pellet, and then into the 270 nm pellet after receiving the first, third, and sixth gel coatings. For any sample in which uptake was measured more than once, the sample was allowed to air dry overnight and was then dried at 110°C for one hour prior to the next uptake experiment. Measurements were made using the apparatus shown schematically in Figure 3. The capillary medium is a high conductivity medium that provides uniform contact across the sample surface. The volume of water imbibed as a function of time was determined from the height change in the graduated capillary tube. Different capillary tube diameters were used depending on the sample pore volume.

Six samples of tuff containing natural fractures were obtained from the Tiva Canyon Member of the Paintbrush Tuff formation in southern Nevada. These samples represent a range of origin (surface and sub-surface), fracture surface mineralization (including manganese oxide, opaline silica, clay minerals and possibly zeolites), and pore structure properties. The tuff samples were cut using a diamond saw to cubes of approximately 1 cm x 1 cm x 1 cm with the undisturbed face being the natural fracture face. The lateral sample sides were sealed with a clear silicone cement. Capillary uptake was measured first into the mineralized fracture face and then into the freshly-cut matrix face on the opposite side of the sample that is parallel with the mineralized fracture face. The apparatus shown in Figure 3 was also used for these experiments.

Each of the sphere compacts and tuff samples were characterized by nitrogen adsorption and scanning electron microscopy (SEM). The sphere compacts and tuff samples were also analyzed via mercury porosimetry, to ascertain the nature of their pore structure. Mercury porosimetry was conducted using a Quantachrome Autoscan-33 scanning porosimeter over the pressure range of 12-33,000 psia, with an assumed contact angle of 140°, and a mercury surface tension of 480 erg/cm^2. Specific surface area was found from BET analysis of nitrogen adsorption isotherms generated using a Quantachrome Autosorb-1 sorption analyzer. Samples were outgassed at 110°C for 3 hours before analysis. Five relative pressure values in the range of 0.05 to 0.3 were used. The nitrogen molecular cross section was taken to be 0.162 nm^2. Physical imaging was conducted using a Hitachi S-800 SEM on gold or platinum coated samples.

RESULTS

Water Uptake by Silica Sphere Compacts

Ordered sphere packings were selected to test the applicability of the experimental procedure because the pore structure is very similar to that implied in the Washburn Equation (i.e., cylindrical, uniform pores) and because the pore geometry/pore size is known from first principles. The degree of sphere and pore size uniformity is evident in the SEM micrograph presented in Figure 4. This micrograph is a fracture cross-section of an ordered packing of 270 nm spheres. These spheres are not perfectly smooth, but have small-scale ($\approx$ 2 nm) surface roughness which leads to nitrogen adsorption surface areas approximately 50% larger than the geometric surface areas. However, this surface roughness has been shown to have negligible effect on capillary uptake [Holt and Smith, 1989].

As predicted by Equation 2, a plot of the volume (V, which is directly proportional to h) of water imbibed versus the square root of time ($t^{1/2}$) should be linear until the sample is saturated. The two V vs. $t^{1/2}$ plots for the sphere packings shown in Figure 5 indicate that this is true. Virtually all the sphere packings exhibit this same straight-line V vs. $t^{1/2}$ behavior. The difference in the volume corresponding to the plateau region for each sample is a result of different sample lengths and pore size, and therefore, different total pore volume.

Note from Equation 2 that the slope of the V vs. $t^{1/2}$ plot is directly proportional to $r^{1/2}/\tau$. Therefore, a value of τ may be calculated from the slopes of these plots since the pore radius is known. Let m be defined to be the slope of the V vs. $t^{1/2}$ plot. For a given packing geometry, τ should be constant, and a plot of m^2 vs. r should be linear and have slope proportional to $1/\tau^2$. The average pore radius, r, for ordered sphere packings can be defined as the hydraulic radius (assuming smooth spheres):

$$r = \left(\frac{2}{3}\frac{\epsilon}{(1-\epsilon)}\right) r_{sphere} \tag{18}$$

The slope of the m^2 vs. r plot for ordered sphere packings, obtained by linear regression, resulted in a τ value of 2.63. This τ value compares reasonably to common theoretical definitions such $1/\epsilon$ [Dullien, 1979] and to measured values for these same porous solids

from Knudsen diffusion of gases [Olague, et al., 1988].

To ascertain the effect of a discrete boundary on the imbibition behavior, capillary uptake experiments were conducted on the two-layered pellet described earlier. As shown in Figure 6, there are two distinct linear regions in the uptake curves, the breakpoint corresponding to the transition from the first region to the second. Although not shown here, the same slopes were obtained for each of the respective two regions regardless of which side absorption was initiated through (only their order was reversed). In addition, the location of the break point was consistent (based on volume imbibed) from one side to the other. What these results indicate is that, for this sample, the presence of region 1 has a negligible impact on the uptake rate in region 2 (that is, aside from delaying the uptake into region 2).

As shown in Figure 6, agreement between the experimental data and the theory predicted by Equation 12 using experimentally determined constants (for porosities, pore radii, tortuosities, etc.) was good. The value used for the permeability in region 1 was estimated using a simple analogy between Darcy's law and Poiseuille's law ($k = \epsilon r^2/8$).

Water Uptake Across Natural and Artificial Fracture Coatings

A series of six tuff samples (herein nominally referred to as tuffs 1-6) were analyzed. Pore structure analysis revealed distinct differences in pore size and structure between each of the tuff samples. Pore size distributions obtained from mercury porosimetry for the four tuff samples which had measurable pore volume (1, 2, 3, and 5) are presented in Figure 7. Two samples (tuff 4 and 6) had no measurable intrusion within the detectable pore size range of the porosimeter (3 nm to 4 μm). The four tuff samples presented in Figure 7 all exhibited fairly broad pore size distributions (PSD's). Tuff 1 exhibited a broad, unimodal PSD with a maximum at 40 nm. Tuff 3 had a bidisperse PSD with maxima at 15 nm and 60 nm. Tuffs 2 and 5 had no clear maximum in the PSD. These differences in pore structure are also reflected in the tuff microstructure as observed by SEM. Figure 8 includes SEM micrographs of rock matrix material from tuffs 1, 2, 3, and 5. Table 1 summarizes the pore structure properties of these four tuff samples. Tuffs 1, 2, 3, and 5 were the only ones used for the capillary rise experiments.

Plots of V vs. $t^{1/2}$ for the tuff samples were surprising with regard to two points. First, linear behavior was noted throughout despite the wide pore size distributions found in some of these samples. This behavior can easily be seen in Figure 9, which presents the volumetric uptake results for tuff 1 through both the mineralized (coated) and non-mineralized (fresh) faces. Linear behavior for this sample is not particularly surprising given its unimodal pore size distribution. However, the fact that similar results were obtained for tuffs 2, 3, and 5 is not fully understood. The second point is, though we see the effects of the mineralized layer as a change of slope, the layer does not effect linearity.

By visual inspection, tuff 1 had the smallest degree of surface mineralization, the natural fracture surface showing only a slight discoloration. Closer observation under an optical microscope indicated the possible presence of clay minerals on the surface. EDS (energy dispersive spectroscopy) surface analysis could not distinguish between the matrix material and the mineralized layer, however. These observations were also true of tuffs 2 and 3. Tuff 5, on the other hand, had a definite, distinct surface covering (identified as opaline silica). The relative effects of this coating are apparent in the uptake curves shown in Figure 10. Linear behavior is observed for uptake through the non-mineralized face with small deviations noted at short and long times. The short time nonlinearity could be the result of the broad pore size distribution of this sample or increased measurement uncertainty resulting from the small pore volume of this sample (note the reduced volume scale). The nonlinearity at long times could be the result of air entrapment due to a relatively impermeable fracture coating. For uptake through the mineralized fracture surface, measurements were at the lower limits of our detection capability. Nevertheless, the dramatic decrease in the uptake rate is readily apparent. Uptake results for tuffs 2 and 3 were intermediate to the two samples illustrated.

Note that for the tuff samples, unlike the two-layered silica sphere sample discussed above, the presence of a coating (region 1) did have an impact on the uptake rate in the matrix (region 2). This is believed to be the result of the very low permeability of the coating (region 1) in the tuff samples. Because the wetting front could be observed moving through each of the tuff samples at a rate consistent with the change in the graduated capillary tube, it is believed that any changes in uptake were not the result of chemical reaction (eg., hydration, hydrolysis, or devitrification) at or near the fracture/matrix interface.

From the slopes of the uptake curves for both faces of a given sample, we can calculate the ratio of an "effective" permeability (which includes the effect of the mineralized layer and the tuff matrix) to the permeability of the matrix alone. This is based on the slopes of the V vs. $t^{1/2}$ plots being proportional to $r^{1/2}$ and the assumption that the permeability is proportional to r^2. These ratios are given for samples 1, 2, 3, and 5 in Table 2. We should note that since we are taking the ratio of experimental slopes to the fourth power, these ratios are only accurate to an order of magnitude. It is evident, nevertheless, that for two of the four samples the mineralized coating on the fracture surface had a significant effect on the rate of matrix uptake. In fact, for tuff 5, the coating dominated the uptake rate by the matrix.

The results of capillary uptake experiment(s) and the uptake curve predicted by the model (Equation 12) into the gel-coated pellet are given in Figure 11. Typical values for the physical parameters of an xerogel [Brinker & Scherer 1990] were used in the model. Again, the observed behavior agrees extremely well with theory, displaying an initial non-linear region followed by a linear region. This was not, however, the observed behavior of the tuffs or the two-layered pellet. The transition from non-linear to linear behavior in region 1 seems to occur (as determined by the model) as the region 1 layer thickness, L_1, increases. Using the physical constants of the model materials, this transition occurs as the layer thickness approaches at ~300 μm. In the tuff samples, L_1 is believed to be very thin and therefore, only the linear uptake behavior in region 2 is observable. Also, the model indicates that the slope of the uptake curve in region 2 is not significantly impacted (i.e., did not decrease, as with the two-layered pellet) as a result of the presence of region 1 until the permeability of region 1 was very low (i.e., less than about 1×10^{-20} m^2). As mentioned earlier, this seemed to be the case with the tuff samples. At intermediate permeabilities (defined here to be about 1×10^{-17} to 1×10^{-19} m^2) there was a noticeable delay in uptake into the second region, but with little change in the uptake rate. This seemed to be the case with the gel-coated pellet.

Since the types of water uptake behaviors described above were observed with both the tuffs and the gel-coated pellet, and tuffs 1, 2, and 3 had no visually observable or distinctive mineral layer, it may be suggested that a discrete layer is not necessary to cause surface resistance but rather only an 'effective' layer due to alteration in the pore structure and pore size at the matrix surface.

Numerical Fracture Flow Experiments

The numerical fracture flow, matrix imbibition experiments were based on the system depicted in Figure 2. This is conservative in the sense that the flow is conceptualized as a plug down a single fracture rather than as a film on the fracture face or flow through a series of fractures. The model is definitely not conservative in that the matrix is assumed to be initially dry throughout the travel path. The model also assumes that the entire fracture face is coated, channeling is not occurring, and that the matrix, coating, and fracture properties do not change along the travel path. The model also assumes that water perfectly wets the rock surface.

Travel depth, plug length, and plug velocity were each calculated as functions of time. Figure 12 indicates that, for the conditions given, a depth of almost 100 m can be reached within less than an hour. Note that the coating permeability in this case is rather low, but is not inconsistent with the range of permeabilities noted earlier. Figure 13 demonstrates, for the same conditions, how the plug length and plug velocity decrease with depth. The plug length initially decreases very rapidly until about 15 m after which it tends to change rather slowly, indicating that, although the travel depth of this plug of water might be quite large, the volume of water at the greater depths may not be significant. Plug velocity decreases in response to changes in plug length and capillary forces in the fracture. Travel depth would be expected to be much greater if the matrix was initially partially saturated.

Figures 14, 15 and 16 demonstrate how the travel depth changes with coating permeability, k, and fracture aperture. Figure 14 indicates that, for each of the coating permeabilities used, travel depth is not appreciable for fracture apertures less than 200 μm. This is primarily the result of the relatively low plug velocities, and therefore long contact times, in apertures that size. Also, as stated earlier, the smaller the fracture aperture, the longer the plug of water it can support through capillary forces. Above 200 μm apertures, however, the coating permeability can have a significant impact on the travel depth. Changes in the mean pore radius of the matrix rock (see Figure 15) or the initial plug length (see Figure 16) did not seem to have a significant impact on the fracture flow behavior.

SUMMARY

A series of capillary rise experiments have been conducted to investigate uptake behavior of water across a low permeability porous layer and into an unsaturated medium. The experiments were conducted on both fabricated model porous media and on natural tuff samples. Although only a small number of tuff samples from a limited location have been studied, it is apparent that the role of the mineralized coating on fracture surfaces can have a significant effect on the migration of water between the fracture and the matrix. The impact this has is a function of many variables including the coating permeability, thickness, porosity, pore size, tortuosity and the nature of the mineralized coating.

A simple model has been proposed to describe the imbibition of water across a fracture coating by the porous matrix. Imbibition is thought to occur as a saturated-unsaturated medium process. The fracture coating is believed to behave as a saturated, very-low-permeability membrane, with the flow through it described by Darcy's law. Subsequent imbibition into the matrix is believed to follow Washburn Equation, unsaturated medium, capillary uptake behavior. The model developed based on this idea is supported by experimental uptake data.

Model runs seem to indicate that the layer permeability and layer thickness have the greatest potential impact on the imbibition behavior. This is probably because, in addition to being important parameters, these parameter values potentially vary over several orders of magnitude.

Numerical fracture flow experiments indicate that, for the very simple fracture flow model chosen, the presence of low-permeability fracture coatings can have a significant impact on the travel depth and travel time of water flowing down fractures.

ACKNOWLEDGMENTS

The authors thank I. Melendez and S. Hietala at UNM/NSF CMEC for performing the mercury intrusion and SEM analyses respectively. The work performed at the University of New Mexico was conducted under Sandia National Laboratories contract No. 42-3931.

NOTATION

A	normal cross sectional area of sample
g	gravitational constant
h	height of capillary rise, fracture aperture
k	specific permeability
L	length of sample in direction of flow
L_p	length of plug of water flowing in fracture
m	slope of V vs. $t^{1/2}$ plot
P	pressure
Q	volumetric flow rate
r	pore radius
R	pore radius/tortuosity
t	time
V	volume
v	velocity
μ	fluid viscosity
σ	surface tension
ρ	density
θ	contact angle
τ	tortuosity factor
ϵ	porosity

REFERENCES

Bixler, N.E., 1985. NORIA - A Finite Element Computer Program for Analyzing Water, Vapor, Air, and Energy Transport in Porous Media. Sandia National Laboratories, SAND84-2057, Albuquerque, NM.

Brinker, J.C. and Scherer, G.W., 1990. Sol-Gel Science, Academic Press, New York, N.Y.

Carlos, B.A., 1985. Minerals in Fractures of the Unsaturated Zone from Drill Core USW G-4, Yucca Mountain, Nye County, Nevada. Los Alamos National Laboratory, LA-10415-MS, Los Alamos, NM.

Carlos, B.A., 1987. Minerals in Fractures in the Saturated Zone from Drill Core USW G-4, Yucca Mountain, Nye County, Nevada. Los Alamos National Laboratory, LA-10927-MS, Los Alamos, NM.

Cederberg, G.A., Greenwade, E., and Travis, B.J., 1987. The Transport of Uranium and Technetium Through the Unsaturated Tuffs, Yucca Mountain, Nevada. in Mat. Res. Soc. Symp. Proc., vol. 84, pp. 703-712.

Crowe, B.M., and Vaniman, D.T., (comps.), 1985. Research and Development Related to the Nevada Nuclear Waste Storage Investigations, January 1-March 31, 1984. Los Alamos National Laboratory, LA-10154-PR, Los Alamos, NM.

Dudley, A.L., Peters, R.R., Gauthier, J.H., Wilson, M.L., Tierney, M.S., and Klavetter, E.A., 1988. Total System Performance Assessment Code (TOSPAC) Volume 1: Physical and Mathematical Bases. Sandia National Laboratories, SAND85-0002, Albuquerque, NM.

Dullien, F.A.L., 1979. Porous Media: Fluid Transport and Pore Structure, Academic Press, New York, New York.

Holt, T.E., and Smith, D.M., 1989. Chem. Eng. Sci., vol. 44, p. 779.

Hopkins, P.L., and Eaton, R.R., 1990. LLUVIA: A Program for One-Dimensional, Steady-State Flow Through Partially Saturated Porous Media. Sandia National Laboratories, SAND88-0558, Albuquerque, NM.

Lin, Y.T., and Tierney, M.S., 1986. Preliminary Estimates of Groundwater Travel Time and Radionuclide Transport at the Yucca Mountain Repository Site. Sinnock, S., ed., Sandia National Laboratories, SAND85-2701, Albuquerque, NM.

Montazer, P., and Wilson, W.E., 1984. Conceptual Hydrologic Model of Flow in the Unsaturated Zone, Yucca Mountain, Nevada. U.S. Geological Survey, Water-Resources Investigations Report 84-4345, Denver, CO.

Olague, N.E., Smith, D.M., and Ciftcioglu, M., 1988. AIChE Journal, vol. 34, p. 1907.

Peters, R.R., Gauthier, J.H., and Dudley, A.L., 1986. Effect of Percolation Rate on Water-Travel Time in Deep, Partially Saturated Zones. Sandia National Laboratories, SAND85-0854, Albuquerque, NM.

Peters, R.R., and Klavetter, E.A., 1988. A Continuum Approach for Water Movement in an Unsaturated Fractured Rock Mass. Water Resources Research, vol. 24, no. 3, pp. 416-430.

Ross, B., 1984. A Conceptual Model of Deep Unsaturated Zones with Negligible Recharge. Water Resources Research, vol. 20, no. 11, pp. 1627-1629.

Spengler, R.W., Chornack, M.P., Muller, D.C., and Kibler, J.E., 1984. Stratigraphic and Structural Characteristics of Volcanic Rocks in Core Hole USW G-4, Yucca Mountain, Nye County, Nevada. United States Geologic Survey, USGS-OFR-84-789, Denver, CO.

Stober, W., Fink, A., and Bohn, E., 1968. J. Colloid Interface Sci., vol. 26, p. 62.

Sykes, M.L., Heiken, G.H., and Smyth, J.R., 1979. Mineralogy and Petrology of Tuff Units from the UE25a-1 Drill Site, Yucca Mountain, Nevada. Los Alamos National Laboratory, LA-8139-MS, Los Alamos, NM.

Szekely, J., Neumann, A.W., and Chuang, Y.K., 1971. J. Colloid Interface Sci., vol. 35, p. 273.

Travis, B.J., Hodson, S.W., Nuttall, H.E., Cook, T.L., and Rundberg, R.S., 1984. Preliminary Estimates of Water Flow and Radionuclide Transport in Yucca Mountain. Los Alamos National Laboratory, LA-UR-84-40, Los Alamos, NM.

Updegraff, C.D., and Lee, C.E., 1991. DCM3D - A Dual-Continuum, 3-D, Groundwater Flow Code for Unsaturated, Fractured, Porous Media. U.S. Nuclear Regulatory Commission, NUREG/CR-5536, Washington, D.C.

Van Brakel, J., and Heertjes, P.M., 1977a. Powder Technology, vol. 16, p. 75.

Van Brakel, J., and Heertjes, P.M., 1977b. Powder Technology, vol. 16, p. 91.

Van Genuchten, M.Th., 1980. A Closed Form Equation for Predicting the Hydraulic Conductivity of Unsaturated Soil. Soil Sci. Soc. Am. J., vol. 44, pp. 892-898.

Wang, J.S.Y., and Narasimhan, T.N., 1985. Hydrologic Mechanisms Governing Fluid Flow in a Partially Saturated, Fractured, Porous Medium. Water Resources Research, vol. 21, no. 12, pp. 1861-1874.

Wang, J.S.Y., and Narasimhan, T.N., 1986. Hydrologic Mechanisms Governing Partially Saturated Fluid Flow in Fractured Welded Units and Porous Non-Welded Units at Yucca Mountain. Sandia National Laboratories, SAND85-7114, Albuquerque, NM.

Washburn, E.W., 1921. The Dynamics of Capillary Flow. Phys. Review, vol. 17, no. 3, pp. 273-283.

Zimmerman, R.W. and Bodvarsson, G.S., 1990. Combined Analytical/Numerical Approaches to Solving Fluid Flow Problems in the Unsaturated Zone at Yucca Mountain, in High Level Radioactive Waste Management, vol. 2, pp. 818-824.

Zimmerman, R.W. and Bodvarsson, G.S., 1989. Semi-Analytical Solutions for Flow Problems in Unsaturated Porous Media. in Multiphase Transport in Porous Media - ASME Conference Proceedings, pp. 23-28.

Table 1. Pore Structure Properties of Tuff Samples

	Sample			
	Tuff 1	Tuff 2	Tuff 3	Tuff 5
Bulk Density (g/cm^3)	1.38	1.51	1.55	2.08
Hg Pore Volume (cm^3/g)	0.209	0.129	0.162	0.028
He True Density (g/cm^3)	2.19	1.63	1.22	2.56
ϵ (based on He Density)	0.368	0.075	0.191	0.186
ϵ (based on Hg Pore Vol.)	0.289	0.194	0.250	0.057
Surface Area (m^2/g)	23.9	4.0	11.2	3.4

Table 2. Ratio of Effective Permeability (Matrix + Coating) to Permeability of Matrix Alone

	Sample			
	Tuff 1	Tuff 2	Tuff 3	Tuff 5
k_{eff} / k_{matrix}	0.3	0.01	0.3	1×10^{-7}

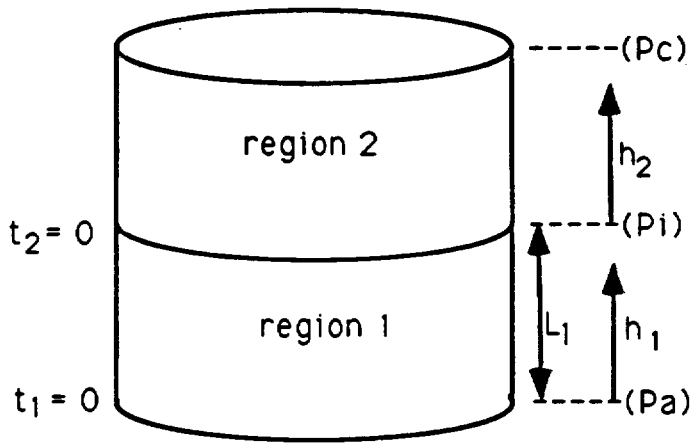

FIGURE 1

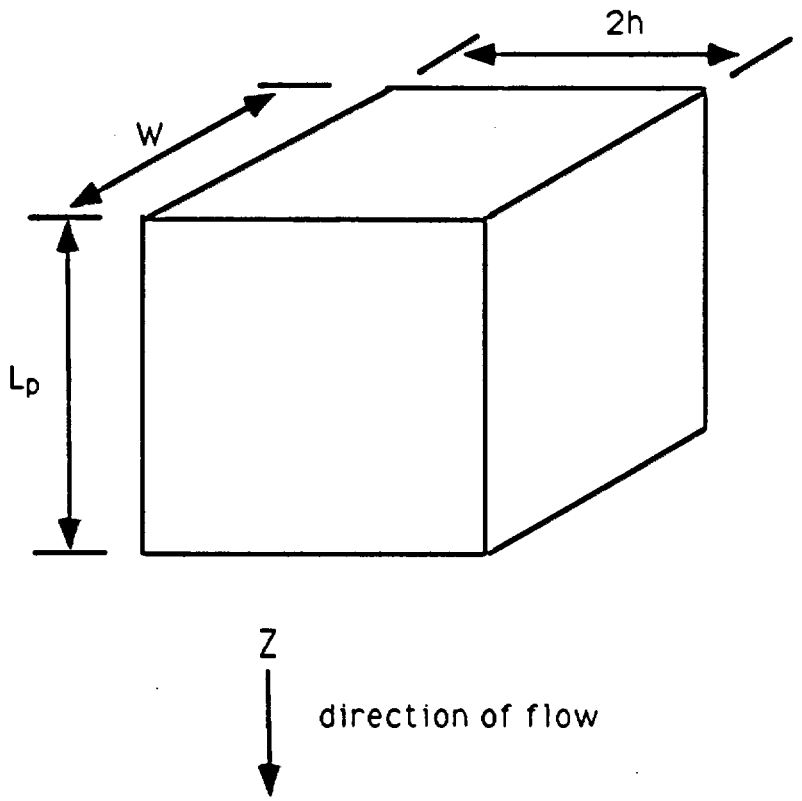

FIGURE 2

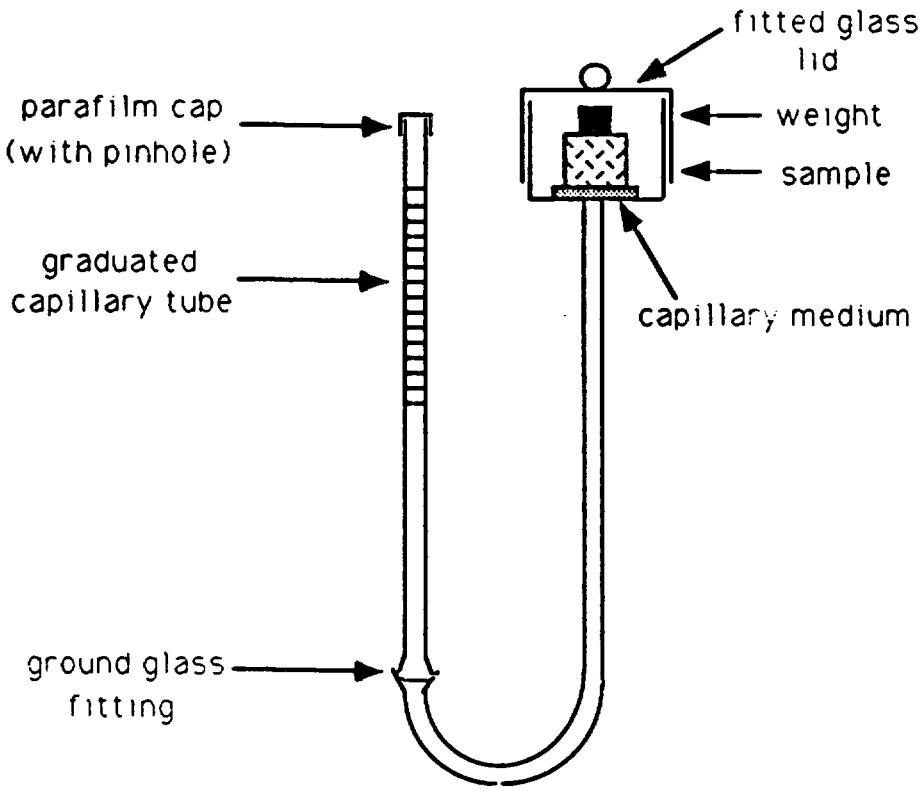
fitted glass
lid
parafilm cap
(with pinhole)
weight
sample
graduated
capillary tube
capillary medium
ground glass
fitting

Figure 3

Figure 4

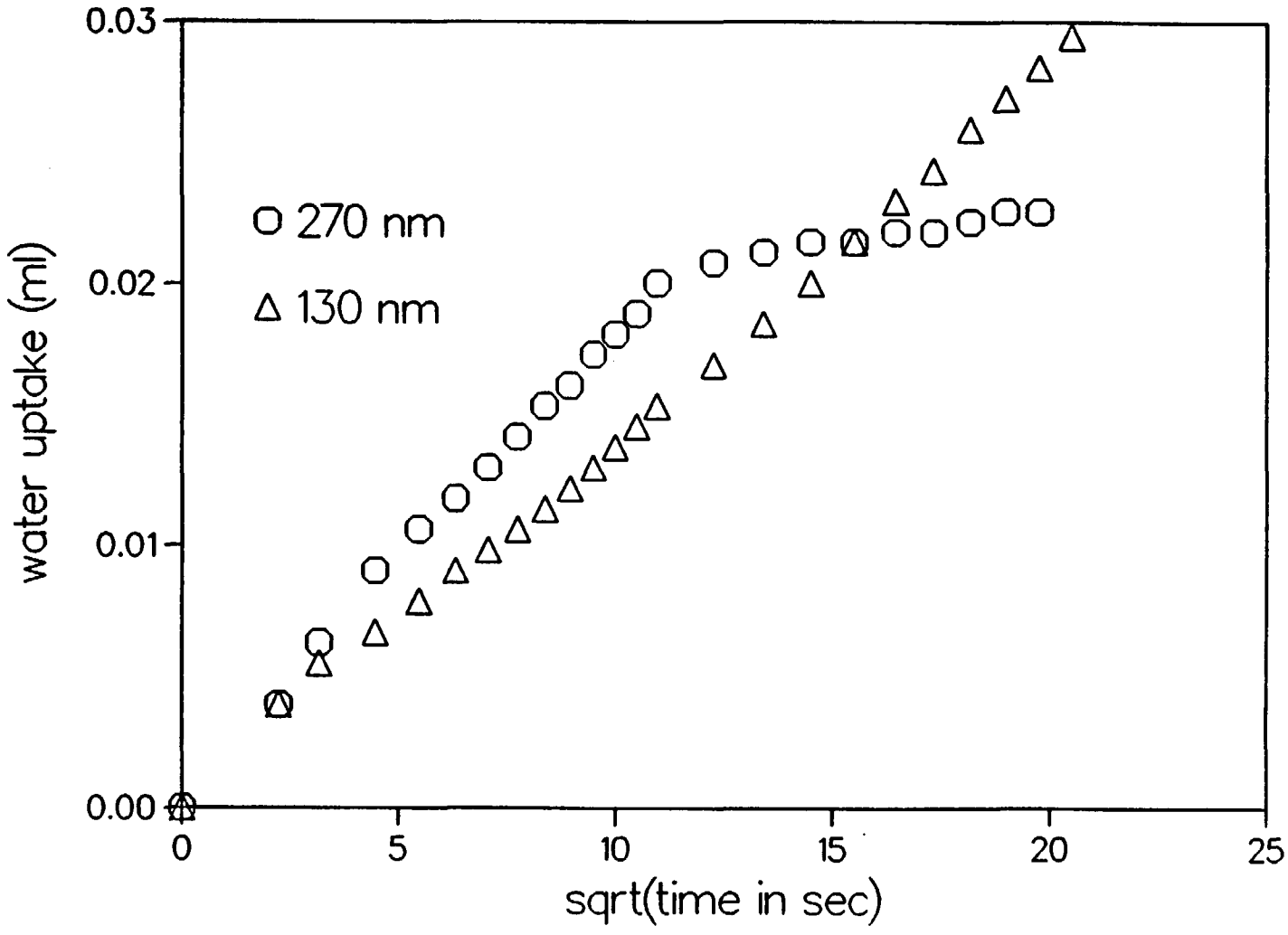
0.03
0.02
0.01
0.00
water uptake (ml)
270 nm
130 nm
0
5
10
15
20
25
sqrt(time in sec)

Figure 5

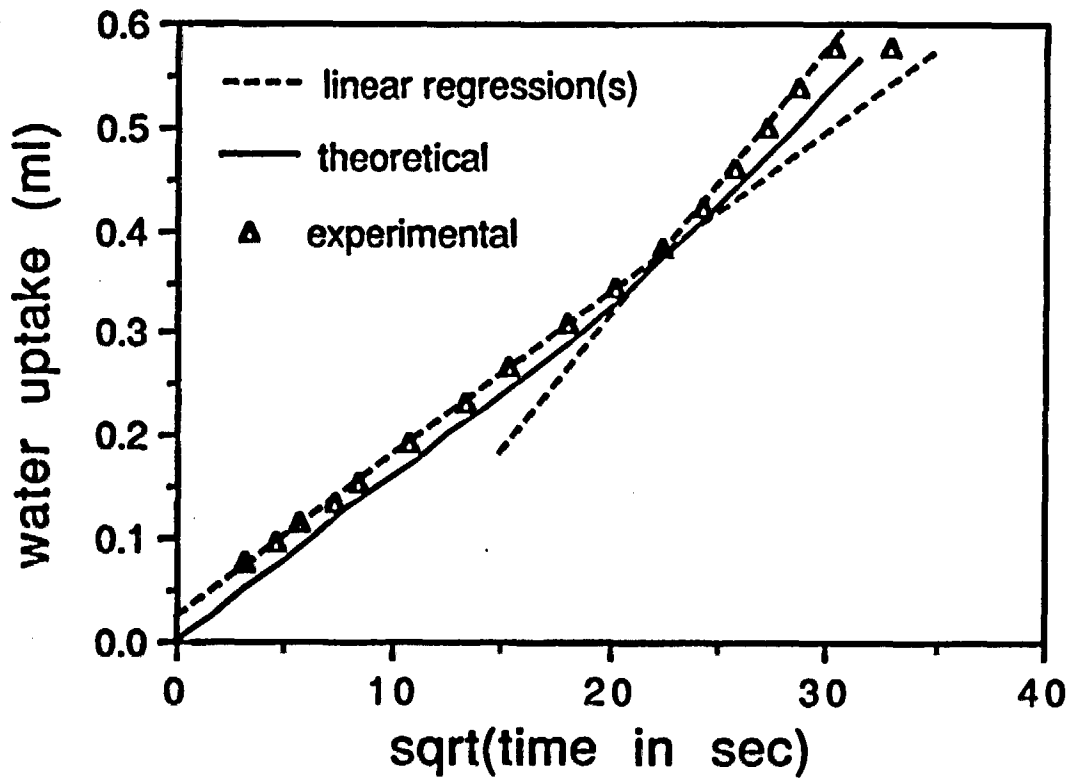
linear regression(s)
theoretical
experimental
water uptake (ml)
0.0
0.1
0.2
0.3
0.4
0.5
0.6
0
10
20
30
40
sqrt(time in sec)

Fig. 6

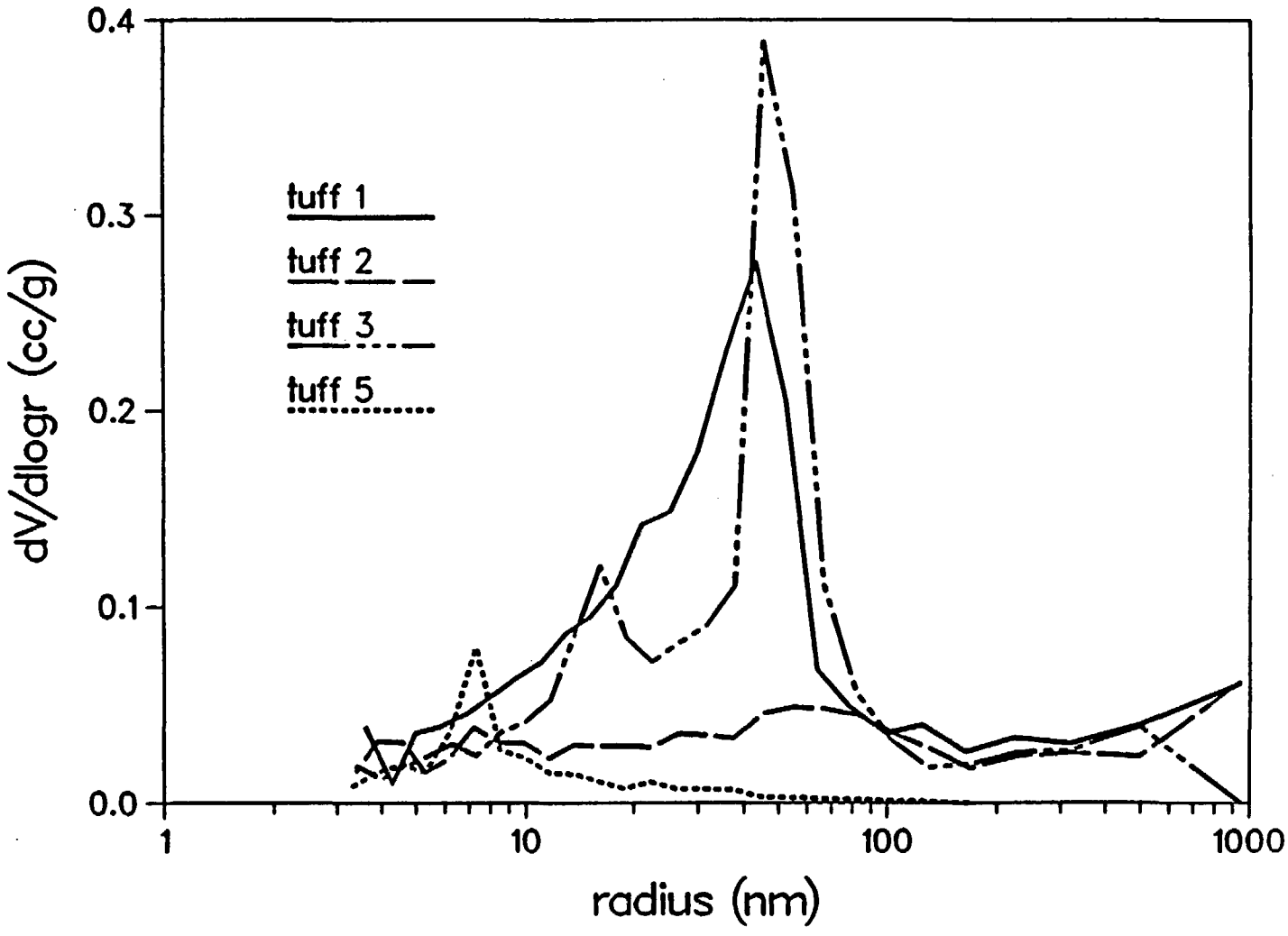
0.4
0.3
0.2
0.1
0.0
dV/dlogr (cc/g)
tuff 1
tuff 2
tuff 3
tuff 5
1
10
100
1000
radius (nm)

Figure 7

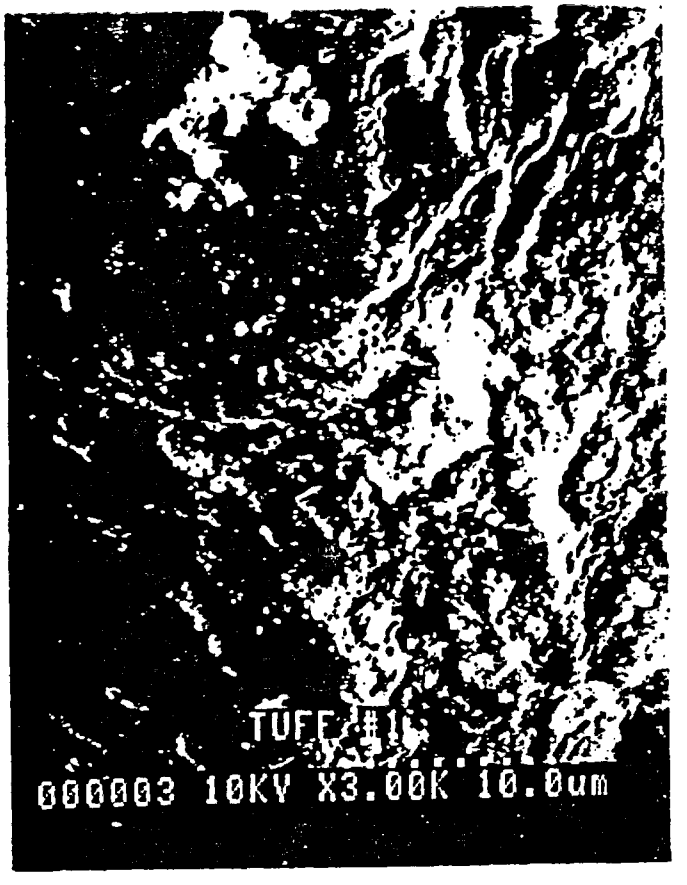
TUFF #1
000003 10KV X3.00K 10.0um

TUFF #2
000001 10KV X3.00K 10.0um

TUFF #3
000002 10KV X3.00K 10.0um

TUFF #5
000001 10KV X3.00K 10.0um

Figure 8

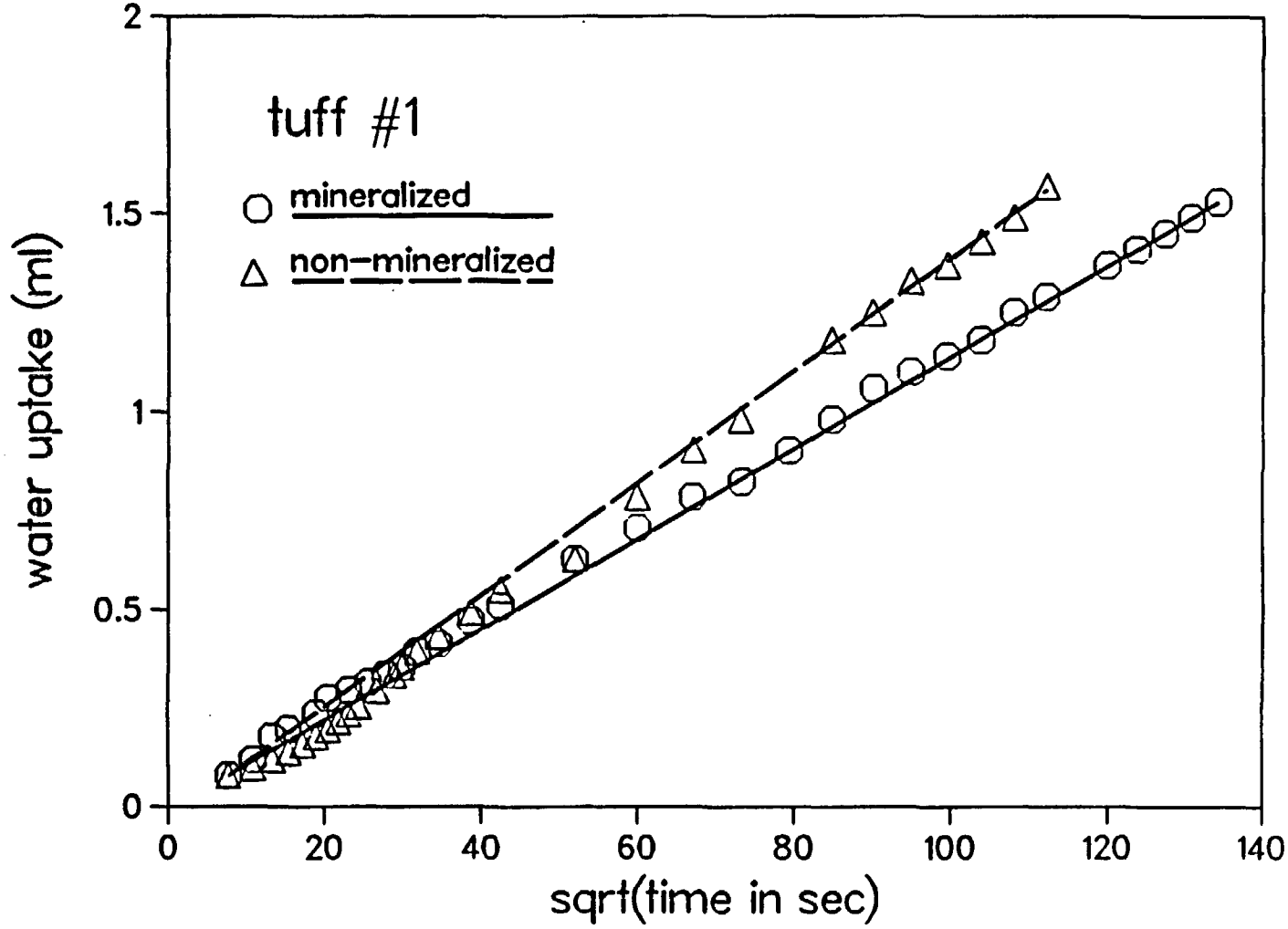
tuff #1
mineralized
non-mineralized
water uptake (ml)
sqrt(time in sec)
0
0.5
1
1.5
2
0
20
40
60
80
100
120
140

Figure 9

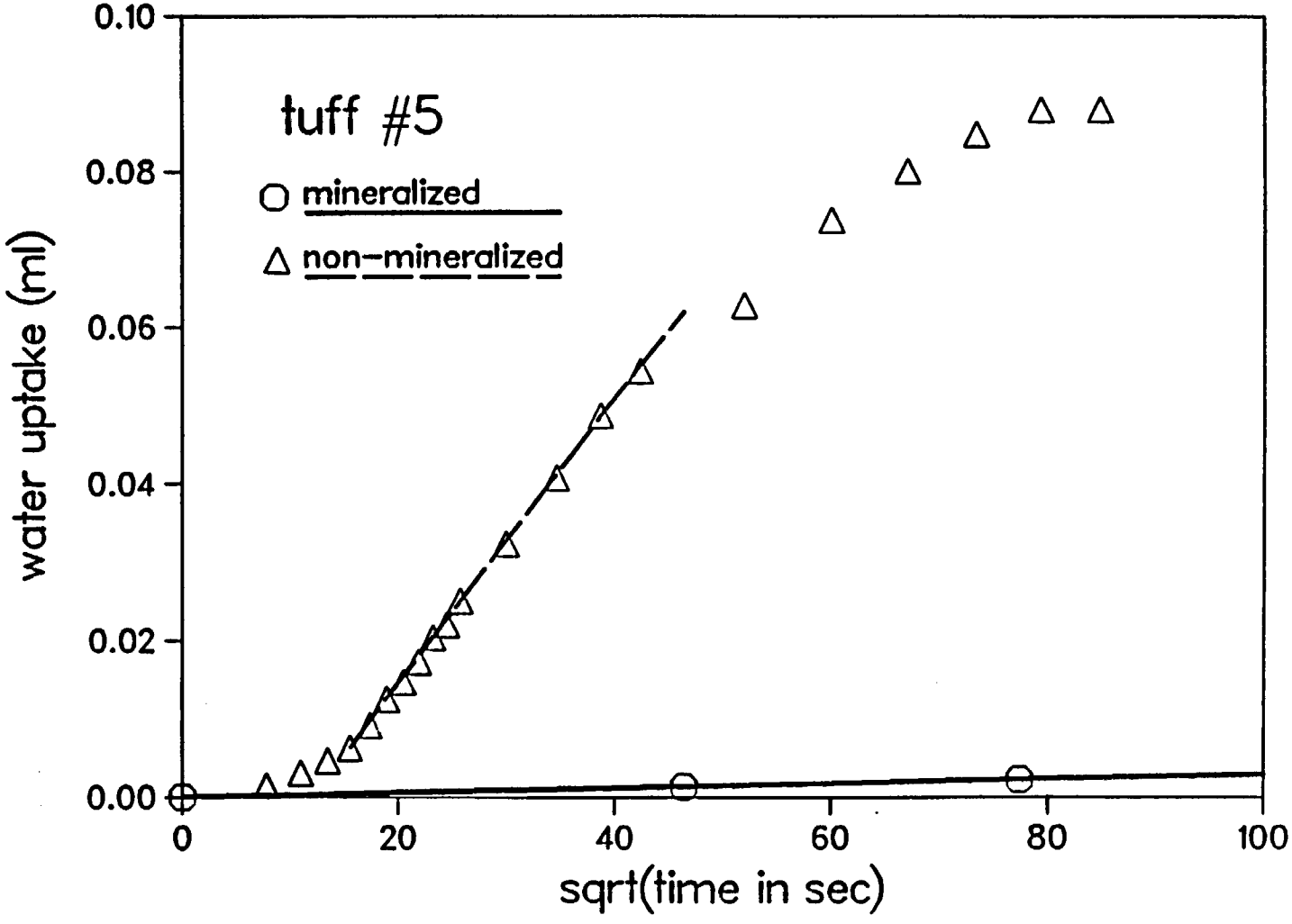
tuff #5
mineralized
non-mineralized
water uptake (ml)
0.10
0.08
0.06
0.04
0.02
0.00
0
20
40
60
80
100
sqrt(time in sec)

Figure 10

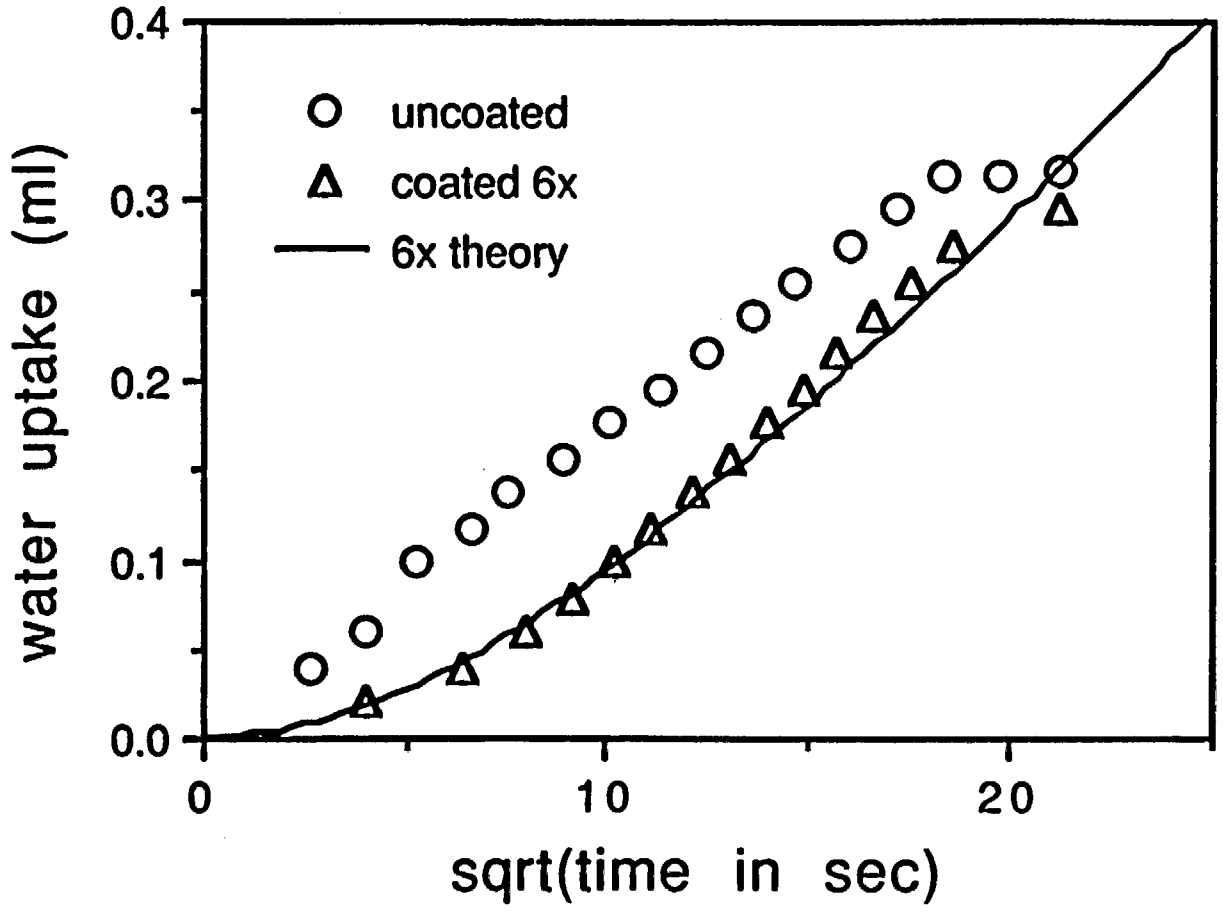
0.4
0.3
0.2
0.1
0.0
water uptake (ml)
uncoated
coated 6x
6x theory
0
10
20
sqrt(time in sec)

Figure 4

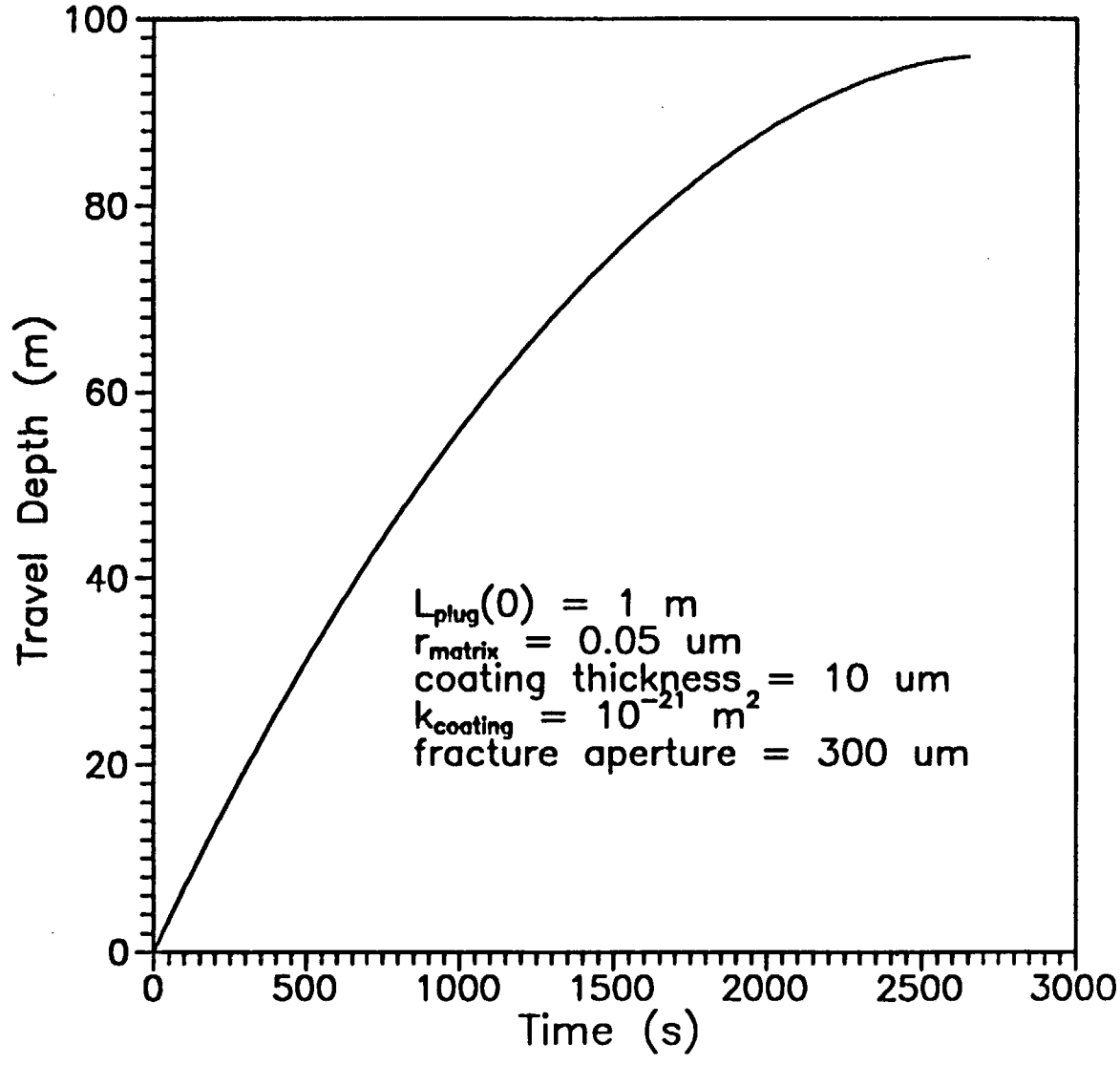
Travel Depth (m)
Time (s)
0
20
40
60
80
100
0
500
1000
1500
2000
2500
3000
$L_{plug}(0)$ = 1 m
r_{matrix} = 0.05 um
coating thickness = 10 um
$k_{coating}$ = 10^{-21} m^2
fracture aperture = 300 um

Figure 12

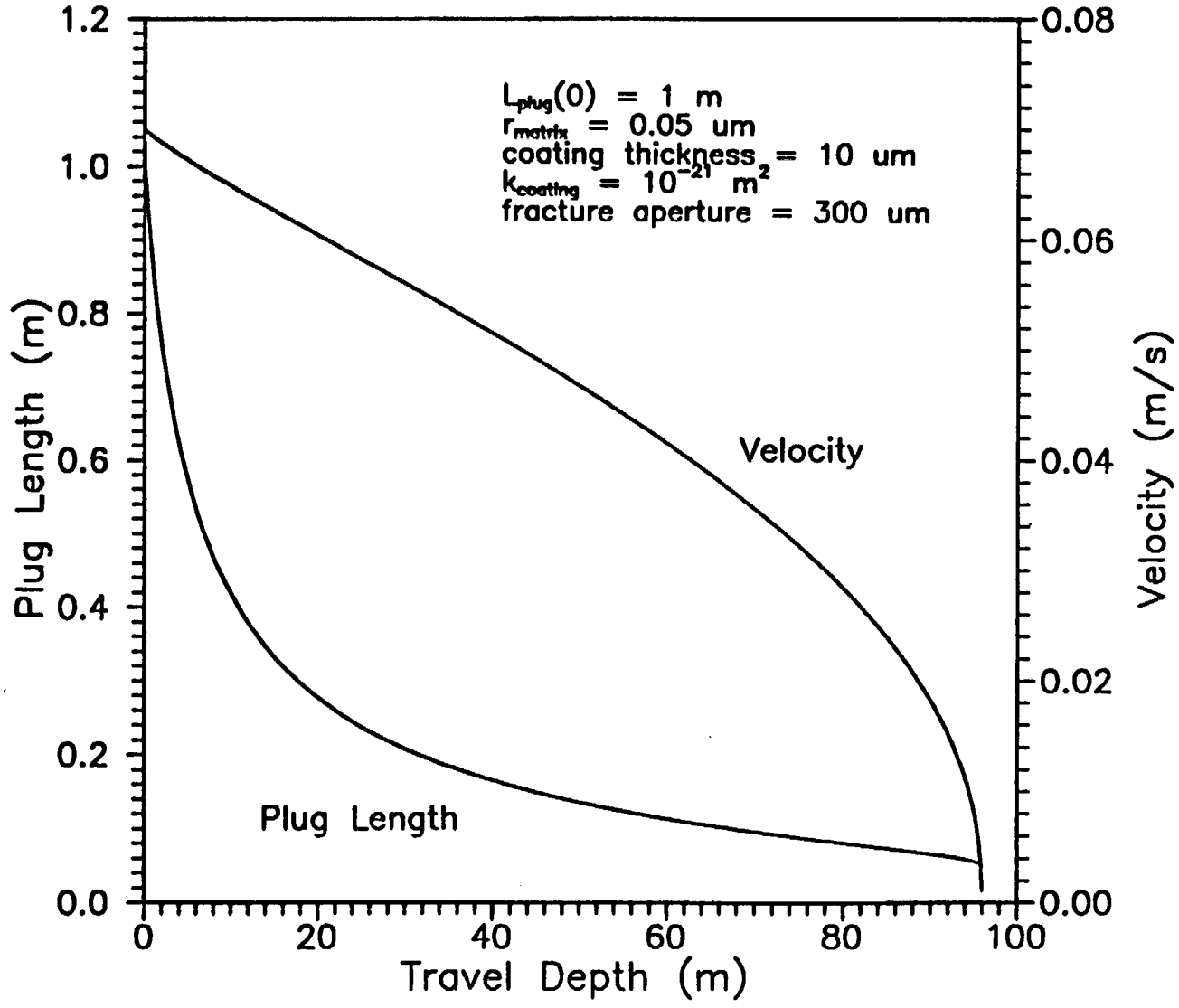
$L_{plug}(0)$ = 1 m
r_{matrix} = 0.05 um
coating thickness = 10 um
$k_{coating}$ = 10^{-21} m^2
fracture aperture = 300 um
Velocity
Plug Length
Plug Length (m)
Velocity (m/s)
Travel Depth (m)
1.2
1.0
0.8
0.6
0.4
0.2
0.0
0.08
0.06
0.04
0.02
0.00
0
20
40
60
80
100

Figure 18

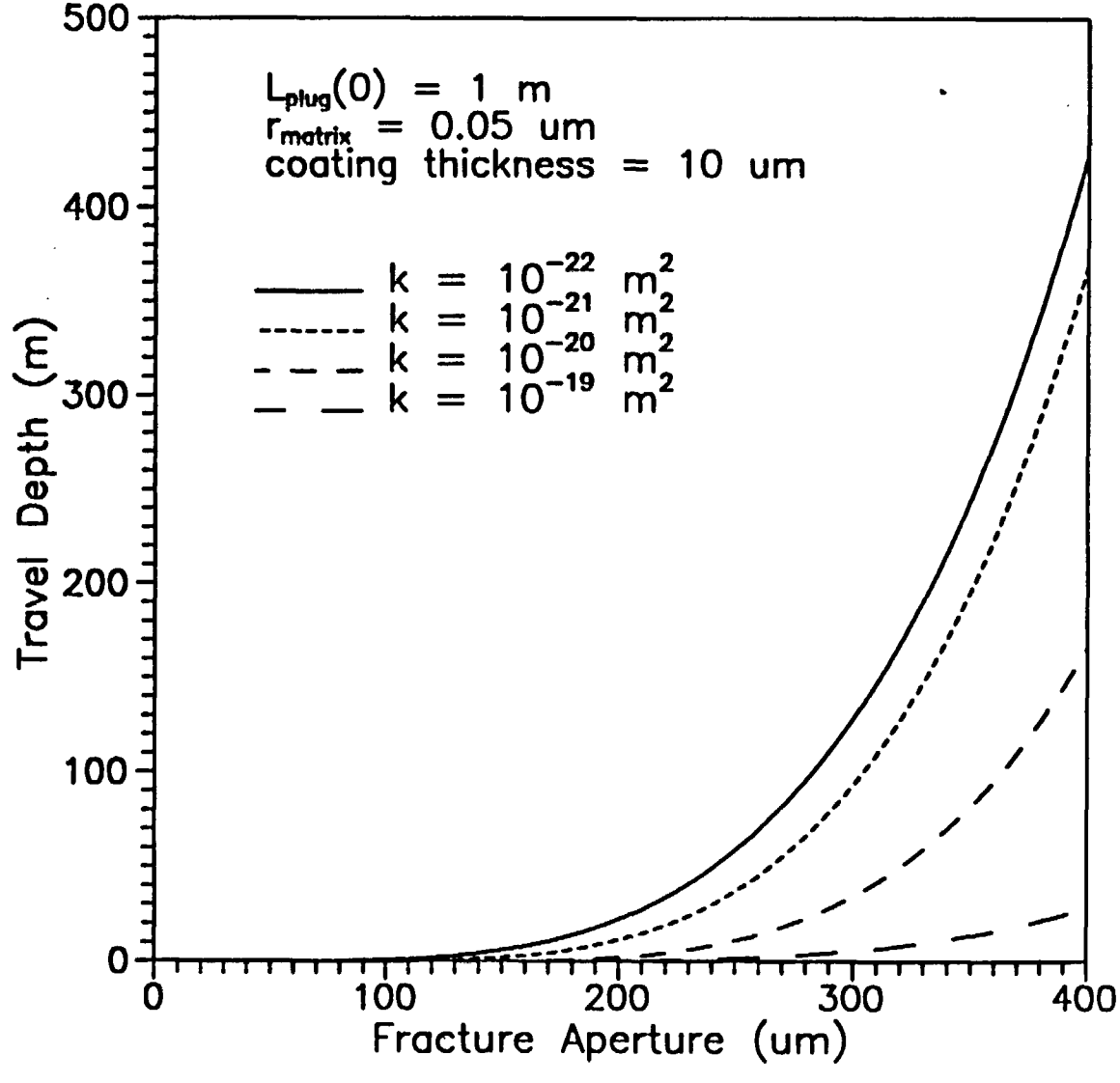
$L_{plug}(0)$ = 1 m
r_{matrix} = 0.05 um
coating thickness = 10 um
k = 10^{-22} m^2
k = 10^{-21} m^2
k = 10^{-20} m^2
k = 10^{-19} m^2
Travel Depth (m)
Fracture Aperture (um)
0
100
200
300
400
500

Figure 14

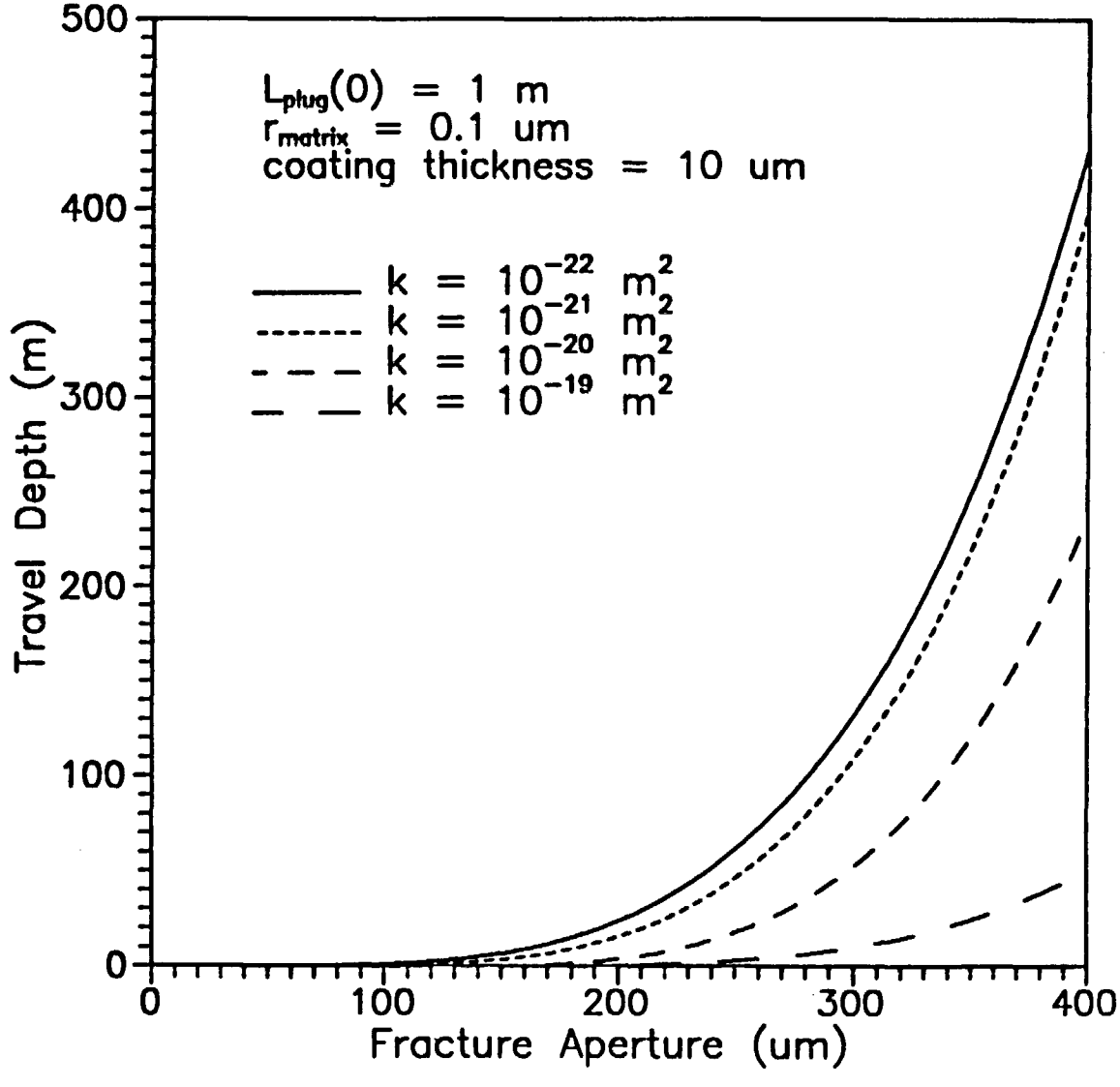
$L_{plug}(0)$ = 1 m
r_{matrix} = 0.1 um
coating thickness = 10 um
k = 10^{-22} m^2
k = 10^{-21} m^2
k = 10^{-20} m^2
k = 10^{-19} m^2
Travel Depth (m)
Fracture Aperture (um)
0
100
200
300
400
500

Fig. 16

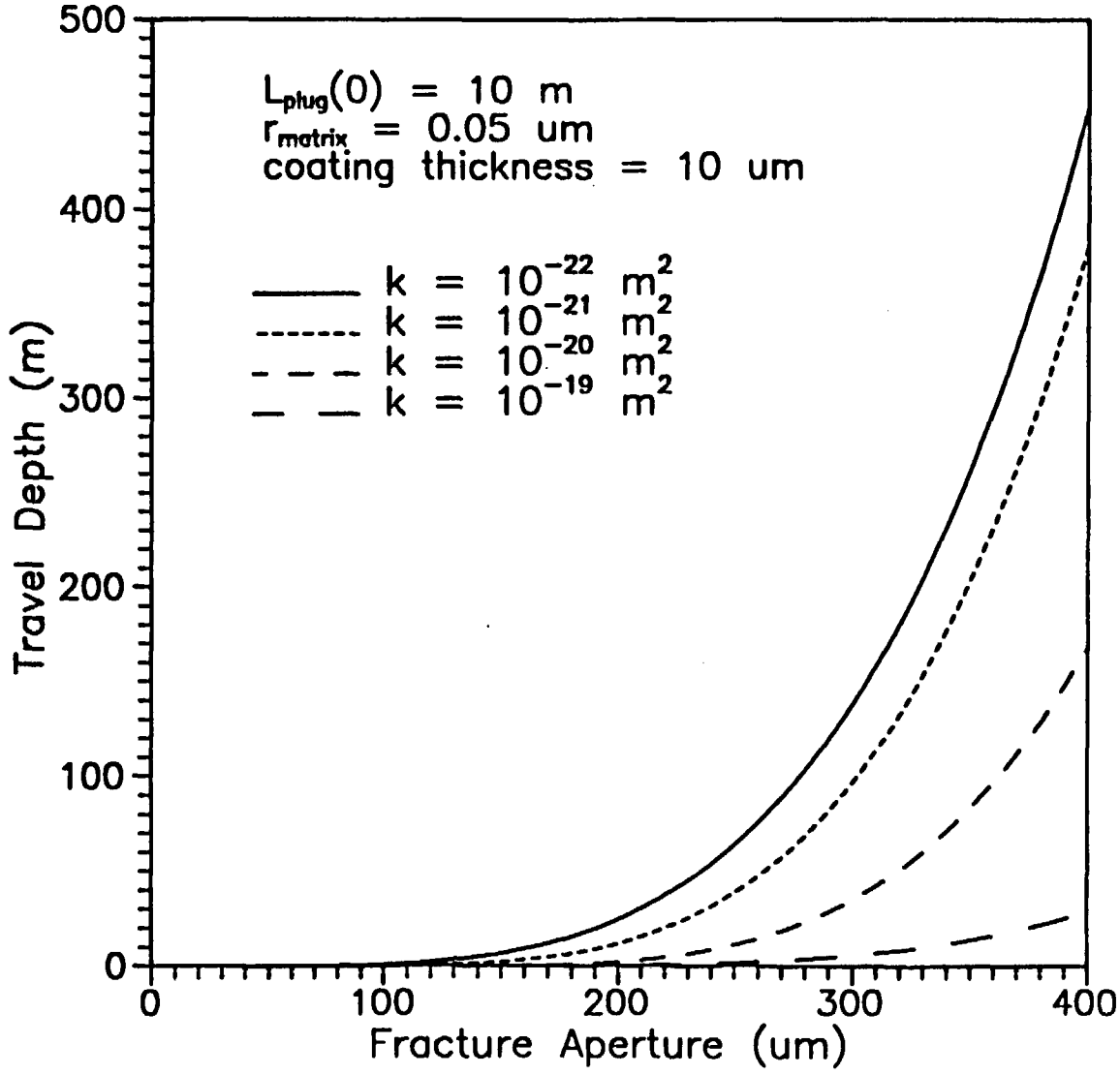
$L_{plug}(0)$ = 10 m
r_{matrix} = 0.05 um
coating thickness = 10 um
k = 10^{-22} m^2
k = 10^{-21} m^2
k = 10^{-20} m^2
k = 10^{-19} m^2
Travel Depth (m)
Fracture Aperture (um)
0
100
200
300
400
500

Figure 16